2013-06-18

Enhanced maximum likelihood grid map with reprocessing incorrect sonar measurements

Lee, Kyoungmin; Lee, Se-Jin; Kölsch, Mathias; Chung, Wan Kyun

Springer

Lee, Kyoungmin, et al. "Enhanced maximum likelihood grid map with reprocessing incorrect sonar measurements." Autonomous Robots 35.2-3 (2013): 123-141.
https://hdl.handle.net/10945/63918

Auton Robot (2013) 35:123–141
DOI 10.1007/s10514-013-9340-5

Enhanced maximum likelihood grid map with reprocessing incorrect sonar measurements

Kyoungmin Lee · Se-Jin Lee · Mathias Kölsch · Wan Kyun Chung

Received: 10 April 2012 / Accepted: 1 June 2013 / Published online: 18 June 2013

Abstract In this paper, we address the problem of building a grid map as accurately as possible using inexpensive and error-prone sonar sensors. In this research area, incorrect sonar measurements, which fail to detect the nearest obstacle in their beamwidth, generally have been dealt with in the same manner as correct measurements or have been excluded from the mapping. In the former case, the map quality may be severely degraded. In the latter case, the resulting map may have insufficient information after the incorrect measurements are removed because only correct measurements are frequently insufficient to cover the whole environment. We propose an efficient grid-mapping approach that incorporates incorrect measurements in a specialized manner to build a better map; we call this the enhanced maximum likelihood (eML) approach. The eML approach fuses the correct and incorrect measurements into a map based on sub-maps generated from each set of measurements. We also propose the maximal sound pressure (mSP) method to detect incorrect sonar readings using the sound pressure of the waves from sonar sensors. In several indoor experiments, integrating the eML approach with the mSP method achieved the best results in terms of map quality among various mapping approaches. We call this the maximum likelihood based on sub-maps (MLS) approach. The MLS map created using only two sonar sensors exhibited similar accuracy to the reference map, which was an accurate representation of the environment.

Keywords Grid mapping · Sonar sensor · Maximum likelihood estimation

1 Introduction

The grid map represents an environment with a discretized field (Thrun et al. 2002). The use of sonar sensors is an attractive approach to building grid maps because of their low cost, ability to detect glass objects (Silver et al. 2004) and insensitivity to light (Hebert 2000). Despite these characteristics, the following troublesome artifacts still exist:

- Erroneous measurements: Lee and Chung (2009) reported that more than 50 % of sonar measurements failed to detect the closest obstacle in general indoor environments due to specular reflection. Because these erroneous measurements hinder accurate map building, most related research (Burguera et al. 2007, 2008; Kuc and Siegel 1987; Leonard and Durrant-Whyte 1992; O'Sullivan et al. 2004; Ivanjko et al. 2003; Lee and Chung 2007, 2009) have focused on the discrimination between correct readings and incorrect ones.
- Inconsistent cells in mapping: Sonar sensors provide range information to the closest obstacle directly, but no

Electronic supplementary material The online version of this article (doi:10.1007/s10514-013-9340-5) contains supplementary material, which is available to authorized users.

K. Lee · M. Kölsch
Department of Computer Science, Naval Postgraduate School, Monterey, CA, USA
e-mail: lekomin@gmail.com

M. Kölsch
e-mail: kolsch@nps.edu

S. Lee
Kyungil University, Gyeongsan, Korea
e-mail: sejiny3@gmail.com

W. K. Chung (✉)
Department of Mechanical Engineering, Pohang University of Science and Technology (POSTECH), Pohang, Korea
e-mail: wkchung@postech.ac.kr

Table 1 Classification of grid-mapping approaches based on their handling of incorrect measurements

Previous approaches	
Incorrect measurements handled in the same way as correct measurements	Posterior approach (Thrun et al. 2002; Ribo and Pinz 2001; Moravec 1988; Thrun 1998) Fuzzy approach (Ribo and Pinz 2001; Oriolo et al. 1997, 1998; Noykov and Roumenin 2007) Dempster–Shafer approach (Ribo and Pinz 2001; Pagac et al. 1998; Murphy 1998; Carlson et al. 2005) Maximum likelihood approach (Thrun 2003; Pathak et al. 2007)
Incorrect measurements discarded	Conflict evaluated maximum approximated likelihood Approach (Lee and Chung 2009)
Proposed new approach	
Incorrect measurements reprocessed	Maximum likelihood based on sub-maps (MLS) Approach: enhanced maximum likelihood (eML) approach + maximal sound pressure (mSP) method

angular information (Choset et al. 2003). When multiple sonar measurements overlap, the angular uncertainty causes inconsistent cells. For example, one measurement might indicate the existence of an obstacle in a certain map cell whereas a second measurement may provide contradictory information. Several estimation approaches (Thrun et al. 2002; Ribo and Pinz 2001; Moravec 1988; Thrun 1998, 2003; Pagac et al. 1998; Murphy 1998; Carlson et al. 2005; Oriolo et al. 1997, 1998; Noykov and Roumenin 2007; Pathak et al. 2007) have been proposed to handle this inconsistency in a reasonable manner.

In addition to these two issues, we found that situations might arise where the correct sonar measurements would not be sufficient to represent the whole environment. In a mapping procedure, incorrect measurements, which fail to detect the nearest obstacle, generally have been treated in the same manner as correct measurements (Thrun et al. 2002; Ribo and Pinz 2001; Moravec 1988; Thrun 1998, 2003; Pagac et al. 1998; Murphy 1998; Carlson et al. 2005; Oriolo et al. 1997, 1998; Noykov and Roumenin 2007; Pathak et al. 2007) or discarded (Lee and Chung 2009; Barshan 2007) to avoid their undesirable effects. Table 1 summarizes several grid-mapping approaches in terms of their handling of incorrect measurements. As shown in Lee and Chung (2009), if incorrect measurements are used in mapping without any special consideration, then the resulting map may contain too many errors to be useful in other applications such as localization or path planning. However, if incorrect measurements are excluded from the mapping process, some areas may not be represented. In the course of several experiments, we found that these situations occur frequently. In particular, the unrepresented areas become quite apparent when only a small number of sonar sensors are used to build the map, as shown in Fig. 1b. If only ideally correct measurements were used, the resultant map could be unsatisfactory.

Based on the consideration that appropriate handling of incorrect measurements and the two issues identified above are fundamental to building high-quality grid maps using error-prone sonar sensors, we propose a new grid-mapping approach called the maximum likelihood based on sub-maps (MLS) approach. The MLS approach consists of two layers: a decision layer and a mapping layer. For the decision layer, we propose the maximal sound pressure (mSP) method to detect incorrect measurements; this is an extension of the concept of using sound pressure proposed in Lee and Chung (2009). For the mapping layer, we propose the enhanced maximum likelihood (eML) approach. The eML approach is based on the maximum likelihood (ML) approach (Thrun 2003; Pathak et al. 2007), because the ML approach is suitable for dealing with inconsistent cells, as described in Sect. 2. However, unlike the ML approach that uses incorrect measurements in the same manner as correct measurements, the eML approach uses a divide-and-conquer strategy to manage incorrect measurements appropriately. The eML approach builds one sub-map for the correct measurements and another for the incorrect measurements, and then merges the two sub-maps into one. Briefly, after collecting the sonar readings, the mSP method divides the readings into two groups: incorrect and correct. The eML approach then builds the final map by merging the two sub-maps.

Our main contributions are as follows:

– To our knowledge, this research represents the first time that incorrect sonar measurements have been considered for sonar grid mapping. The technique of handling incorrect measurements may be extended to building a map using only a few sonar sensors, because incorrect

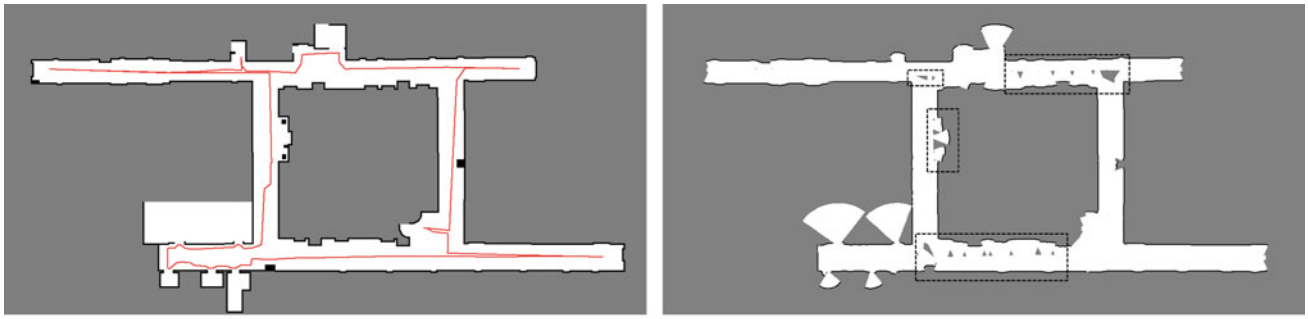

Fig. 1 Example of using only ideally correct measurements obtained from a real indoor experiment. The *white* region represents the empty space, and the *black* region indicates the occupied area. The gray region means the unknown area. **a** Reference map (62 m × 30 m). The *line* indicates the robot trajectory. **b** Grid map based on ideally correct measurements from only two sonar sensors. Correct measurements were extracted from the decision process based on the reference map in (**a**). The extraction is perfect and similar to that of an ideal decision maker for correctly executed measurements. Ideally correct measurements are used, but the map contains unrepresented areas indicated by *dashed boxes*

measurements can compensate for areas that cannot be represented by correct measurements alone. In Sect. 7, we show the results of using a complete 360° band of sonar sensors and results using only two sonar sensors. For reasons of cost, a small number of sonar sensors is desirable for commercial devices, such as robotic vacuum cleaners.

– In general cases, such as when sonar sensors are installed to provide full 360° coverage around a robot, the decision performance of the MLS approach is slightly better than that of the conflict evaluated maximum approximated likelihood (CEMAL) approach (Lee and Chung 2009), which has the best performance among various decision methods developed so far. For the case of using only two sonar sensors, the decision performance of the MLS approach is approximately 8 % better than the CEMAL approach. Overall, compared with previous decision approaches (Burguera et al. 2008; Kuc and Siegel 1987; Leonard and Durrant-Whyte 1992; O'Sullivan et al. 2004; Ivanjko et al. 2003; Lee and Chung 2007, 2009; Burguera et al. 2007), the MLS approach is the best for classifying the state of measurements.
– Based on a criterion given in Sect. 7, we confirmed that the number of wrongly represented regions in the MLS map was smaller than in maps built using previous mapping approaches (Thrun et al. 2002; Ribo and Pinz 2001; Moravec 1988; Thrun 1998, 2003; Pagac et al. 1998; Murphy 1998; Carlson et al. 2005; Oriolo et al. 1997, 1998; Noykov and Roumenin 2007; Pathak et al. 2007; Lee and Chung 2009), both when using a complete 360° band of sonar sensors and when using only two sonar sensors.
– The MLS approach has a light $O(n)$ computational load that is comparable to independent estimation approaches (Thrun et al. 2002; Ribo and Pinz 2001; Moravec 1988; Thrun 1998; Pagac et al. 1998; Murphy 1998; Carlson et al. 2005; Oriolo et al. 1997, 1998; Noykov and Roumenin 2007), which are described in Sect. 2, and is very low compared to the $O(n^2)$ load of the CEMAL approach and the $O(2^k n)$ load of the ML approach where n is the number of sonar measurements and k is the number of cells. Additionally, although the MLS approach is based on the ML approach, the MLS solution globally maximizes the likelihood of the measurements.
– The MLS approach does not require adjustment of parameters, unlike independent estimation approaches that must carefully regulate their own update parameters to create accurate maps. The MLS approach requires partial modification only when using a different kind of sonar sensor.

It should be noted that we assumed that pose estimations were available because localization during mapping was not a concern in this study. Even if accurate localization were provided, exact grid-mapping with sonar sensors is still a serious problem due to troublesome artifacts of sonar sensors, and is still demanded for an inexpensive sensor-based application (Choi et al. 2011; Lee and Chung 2010; Burguera et al. 2009a). The pose estimations rely on extended Kalman filter-based simultaneous localization and mapping (SLAM) (Ahn et al. 2008).

The remainder of the paper is organized as follows. We begin by describing related research in Sect. 2. Section 3 provides preliminary definitions, and Sect. 4 presents the mSP method. Section 5 describes the eML approach and Sect. 6 summarizes the MLS approach. Section 7 describes the experimental results and Sect. 8 presents the summary and conclusions.

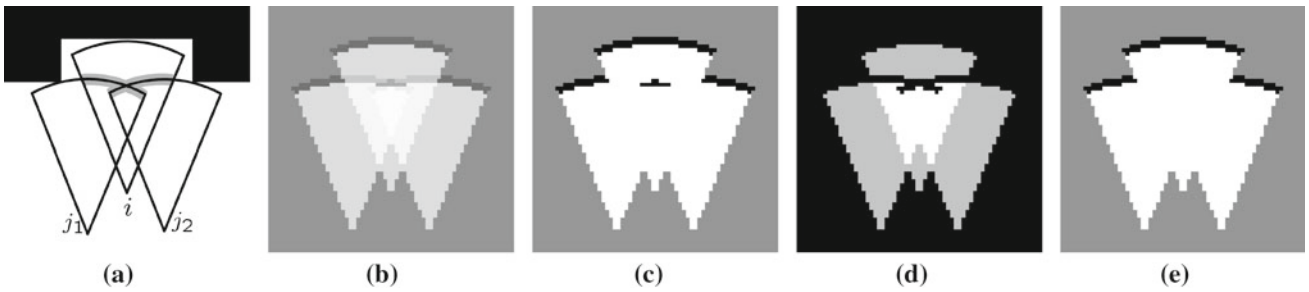

Fig. 2 **a** Three correct sonar readings with inconsistent cells shaded in gray. **b** Posterior approach. **c** Dempster–Shafer approach. **d** Fuzzy approach. **e** Maximum likelihood approach

2 Related works

2.1 Handling inconsistent cells

As mentioned in Sect. 1, handling inconsistent cells is an issue in grid mapping with sonar sensors. Previous research in this area can be classified into two categories: independent estimation and dependent estimation.

- Independent estimation: Independent estimation approaches tackle the inconsistent cell with the assumption that each cell is independent of the others (Thrun et al. 2002). The assumption reduces the problem to finding a solution among 2^k possible maps into a collection of binary or trinary estimation problems.
  - Posterior approach (PT): The PT was proposed for managing the inconsistency with the concept of probability (Thrun et al. 2002; Ribo and Pinz 2001; Moravec 1988; Thrun 1998) and measures the occupancy of the cell.
  - Dempster–Shafer approach (DS): Based on the concept of ignorance, the DS (Ribo and Pinz 2001; Pagac et al. 1998; Murphy 1998; Carlson et al. 2005) infers a belief function that indicates whether a cell is occupied, empty, or in an unknown state based on the Dempster–Shafer theory (Shafer 1976).
  - Fuzzy approach (FZ): The FZ (Ribo and Pinz 2001; Oriolo et al. 1997, 1998; Noykov and Roumenin 2007) quantifies the possibility that indicates a cell belongs to an obstacle. It is based on the theory of fuzzy sets (Zadeh 1973) designed to deal with vagueness, and determines safe cells that are free of obstacles.
- Dependent estimation: Unlike the independent estimation approaches, the maximum likelihood (ML) approach (Thrun 2003; Pathak et al. 2007) does not assume the independence of other cells. The ML map is obtained by maximizing the likelihood of sonar measurements.

The assumption of independence has a serious effect on the quality of the map. As shown in Fig. 2b–d, independent estimation approaches fail to represent the shaded gray region of Fig. 2a, which contains inconsistent cells. In other words, the angular uncertainty of sonar sensors is not appropriately handled by the assumption of independence. Thus, a map built by independent estimation approaches may be defective in terms of representing narrow openings.

Conversely, as illustrated in Fig. 2e, the ML approach represents narrow regions quite accurately. If the state of the cells in the shaded gray region of Fig. 2a is set to occupied, the likelihood of other readings j_1 and j_2 decreases. Thus, the state should be empty to prevent this decrease, and this process makes the ML approach suitable for handling the angular uncertainty of the sonar sensor. We started our research with the ML approach because of its suitability for dealing with inconsistent cells.

2.2 Detecting incorrect measurements

Several techniques have been developed for filtering out incorrect measurements, and these can be divided into five classes.

- By clustering: The random sample consensus/Gaussian filtering (RANSAC/GF) method (Burguera et al. 2008) rejects readings that do not fit a Gaussian distribution established by RANSAC clustering (Fischler and Bolles 1981).
- By geometric primitives: The region of constant depth (RCD) matching method (Kuc and Siegel 1987; Leonard and Durrant-Whyte 1992) extracts readings that satisfy a geometric constraint, based on the radius of a circle. The feature prediction (FP) method (O'Sullivan et al. 2004) discriminates reliable measurements by assigning a confidence measure to each sonar reading, and the measure is determined by hypothetical obstacles.
- By adaptive range: The bounding box method (Ivanjko et al. 2003) reduces the range of measurements that are outside the border created by four adjacent (front, back,

left, right) sensor readings. In the navigable Voronoi diagram (NVD) method (Lee and Chung 2007), the diagram is generated by instantaneous measurements, and sonar readings beyond the diagram are excluded.
– By consistency: The sonar probabilistic analysis of conflicts (spAC) method (Burguera et al. 2007) iteratively determines the probability of each sonar reading, based on the occurrence of conflict cells. The conflict evaluation with sound pressure (CEsp) method (Lee and Chung 2009) determines incorrect measurements through a comparison of sound pressures when conflict cells occur.
– By learning: The neural network learning (NN) method (Thrun et al. 2002) trains a neural network by supervised learning and then determines the status of a measurement.

The mSP method proposed in this paper is not included in the five categories above. It determines the status of the sonar readings using a temporary map based on sound pressure as described in Sect. 4.

3 Definitions

A sonar sensor emits a wave, and the wave returns to the sensor after striking one or several obstacles. The distance to the obstacle is calculated from the time of flight of the wave. Thus, the distance measurement gives information about two regions (Fig. 3): the arc region and the free region. The arc region, where obstacles are most probably located, is the farthest area of the measurement. The free region in which no obstacles exist, is everywhere else in the beamwidth of the measurement except for the arc region.

Sonar sensors were originally designed to provide the distance to the closest obstacle in their beamwidth. When, therefore, a range measurement does not indicate the nearest obstacle, it is incorrect. Conversely, the measurement is correct when it does indicate the closest obstacle. It can be expressed by

$$C(i) = \begin{cases} \text{Correct} & \text{if} \quad \left|z_i - d\left(N\big|_M^{z_i}\right)\right| \le \beta \\ \text{Incorrect} & \text{if} \quad \left|z_i - d\left(N\big|_M^{z_i}\right)\right| > \beta \end{cases} \tag{1}$$

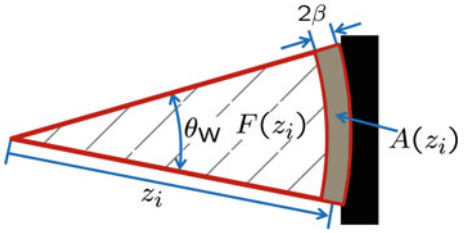

Fig. 3 Region of sonar reading i where θ_w is the beam-width, z_i is the range, $F(z_i)$ is the free (hatched) region, $A(z_i)$ is the arc (*gray*) region, and 2β is the interval corresponding to range uncertainty

where z_i is the range of a sonar measurement and i is the index of the measurement. β indicates range uncertainty and $N\big|_M^{z_i}$ is the nearest obstacle or the nearest occupied cell within the beamwidth of measurement i on a map M. The $d\left(N\big|_M^{z_i}\right)$ is the distance from the sensor to the nearest obstacle, and is defined as

$$d\left(N\big|_M^{z_i}\right) = \begin{cases} \text{distance to } N\big|_M^{z_i} & \text{for} \quad N\big|_M^{z_i} \neq \varnothing \\ z_{max} & \text{for} \quad N\big|_M^{z_i} = \varnothing \end{cases} \tag{2}$$

where z_{max} is the maximum detectable range. The $N\big|_M^{z_i}$ corresponds to the nearest obstacle in the real environment, or the closest occupied cell on a map.

4 Decision—maximal sound pressure method

We build a temporary map based on the sound pressure to classify a sonar reading into one of two groups: incorrect or correct.

4.1 Sound pressure

A sonar sensor emits a wave that returns to the sensor after hitting an obstacle. The distance to the obstacle is calculated from the time of flight of the wave. The pressure of the returning wave on the sensor is called the sound pressure (Lee and Chung 2009), and is expressed as

$$SP(r,\theta) = \frac{1}{r} 10^{\frac{D_T(\theta)+D_R(\theta)}{20}} \tag{3}$$

where r is the distance from the sensor to the obstacle, θ is the angle from the heading of the sensor, $D_T(\theta)$ is the transmitting directivity, and $D_R(\theta)$ is the receiving directivity (Kleeman and Kuc 2008). The parameters $D_T(\theta)$ and $D_R(\theta)$ depend on the specific characteristics of the sonar sensor being used. The derivation of (3) is provided in Lee and Chung (2009).

The log function is introduced for computational reasons and (3) can be simplified to

$$LSP(r,\theta) = \frac{D_T(\theta) + D_R(\theta)}{20} - \log r. \tag{4}$$

Because one sound pressure is compared with another sound pressure, the use of the log function does not affect the result of the comparison.

We used two well-known sonar sensors: the 600 series from SensComp Inc. (S600) and the MA40B8 from Murata Co., Ltd (MA40B8). After applying the specific $D_T(\theta)$ and $D_R(\theta)$ from each sensor, the final sound pressure levels were

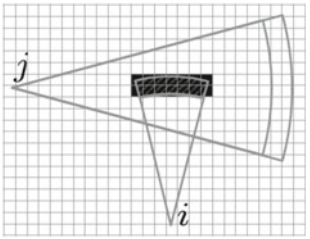

Fig. 4 The black cells are conflict cells. In this case, the whole arc region of the measurement i is included in the free region of the other measurement j. Thus, the information supported by reading i is contradicted by the information supported by reading j

– S600 ($|\theta| \leq 11.25°$)

$$LSP(r,\theta) = -0.00605\theta^2 - 0.01977|\theta| - \log r \quad (5)$$

– MA40B8 ($|\theta| \leq 22.5°$)

$$LSP(r,\theta) = -0.001025\theta^2 + 0.00147|\theta| - \log r. \quad (6)$$

4.2 Conflict evaluation with sound pressure (CEsp) method

Inconsistency of information contained in cells may occur when multiple sonar measurements overlap. Depending on the inconsistency, a cell may be classified into one of two groups: consistent cells C_c and inconsistent cells I_c. Additionally, inconsistent cells are further classified into two other groups: uncertain cells U_c and conflict cells F_c. The conflict cells occur when all of the arc cells of a measurement are on the free regions of other measurements (Fig. 4). Details about other types of cells such as the consistent cell and the uncertain cell are provided in Lee and Chung (2009). There are always incorrect measurements when conflict cells occur; this was shown in Lee and Chung (2009). Based on this, the CEsp method (Lee and Chung 2009) determines incorrect measurements through the comparison of sound pressures in conflict cells.

Although incorrect measurements are always included in the case when conflict cells occur, not all incorrect measurements cause conflict cells. Thus, determining incorrect measurements only when conflict cells exist may limit the determination of all incorrect measurements. Therefore, we propose a new decision method to cover the case when conflict cells do not occur.

4.3 Maximal sound pressure (mSP) method

The sound pressure comparison is applied to only conflict cells in the CEsp method. Unlike the CEsp method, however, we extend the application of the comparison to all cells covered by all sonar readings. The result of the comparison

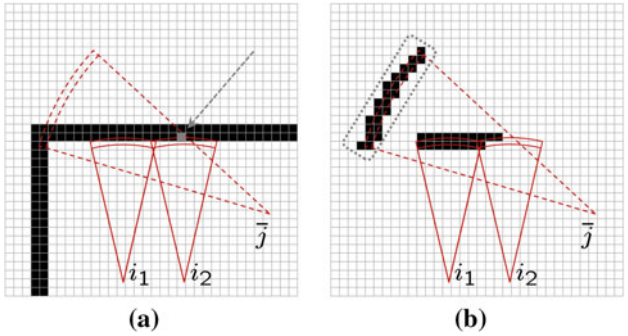

Fig. 5 Example of the mSP map and the decision procedure based on that map: **a** environment on a gridded field and three sonar measurements i_1, i_2, and $\bar{j}$. The *arrow* indicates a cell for instantiating the notation used in (8). **b** The mSP map built based on three readings. The *dotted box* indicates the erroneous outside area. Based on the mSP map, reading $\bar{j}$ contains some obstacles in its free region, and thus it becomes the incorrect measurement

is represented by a temporary map $\widehat{M}$, called the maximal sound pressure (mSP) map. The mSP map is obtained using

$$\widehat{M} \equiv \left\{ M \middle| O_c(M) = \bigcup c^*_{xy} \right\} \quad (7)$$

where M is the map, and $O_c(M)$ is all occupied cells in M. (7) indicates that the mSP map flags only specific cells c^*_{xy} as occupied where c^*_{xy} is defined as

$$c^*_{xy} \equiv \left\{ c_{xy} \middle| \mathbf{max}\left(LSP_P(c_{xy})\right) > \mathbf{max}\left(LSP_N(c_{xy})\right) \right\} \quad (8)$$

where c_{xy} is a cell, $LSP_P(c_{xy})$ is the sound pressure of the measurement that indicates there may be an obstacle in cell c_{xy}, and $LSP_N(c_{xy})$ is the sound pressure of the measurement that indicates there are no obstacles in the cell c_{xy}.

For example, for the gray cell in Fig. 5a, $LSP_P(c_{xy})$ is obtained from measurement i_1, because the reading i_1 indicates that there is an obstacle in the cell. Additionally, because the reading $\bar{j}$ indicates there are no obstacles in the cell, $LSP_N(c_{xy})$ is calculated from the reading $\bar{j}$.

Figure 5b shows an example of the mSP map for the case of Fig. 5a. As shown in Fig. 5b, the areas outside the boundary of the environment contain errors while areas inside the boundary are defined reliably. This feature of the mSP map is due to taking obstacle information from the reading with the highest sound pressure. More specifically, because the sound pressure has a higher value for an obstacle closer to the sensor and closer to the sensor's line of the sight, we consider the information with the highest sound pressure to be true. The clean inside representation property of the mSP map means it can be used as a standard to determine the status of measurements, but not be used as a map due to erroneous outside areas.

(1) is applied to a measurement using the mSP map to determine the status of that measurement. For example, in

Fig. 5b, the measurement $\bar{j}$ is determined to be an incorrect reading, because it includes some occupied cells that indicate obstacles in its free region. The complexity of building the mSP map is $O(n)$ because the mSP map is generated with a complexity proportional to the number of measurements. The decision complexity is also linear to the number of measurements. The total computational complexity is $O(n)$, i.e., $O(n+n)$. The decision based on the mSP map and (1) is called the maximal sound pressure (mSP) method.

As will be shown in Sect. 7, the mSP method gives better results than previous decision methods, especially when only two sonar sensors are used. This is because the mSP method works without considering whether conflict cells occur. Thus, even in the case when there are insufficient relationships among sonar readings, the mSP method will still determine the status of measurements reliably.

In this section, we have described how all sonar readings are classified into two groups. In the next section, based on the classification, we explain how the grid map is made.

5 Mapping—enhanced maximum likelihood approach

The enhanced maximum likelihood (eML) approach proposed in this paper starts with the ML approach, due to its effectiveness in handling inconsistent cells as described in Sect. 2.

5.1 Previous maximum likelihood approach

5.1.1 Maximum likelihood (ML) approach

Because sonar sensors are designed to measure the range to the closest obstacle in their beamwidth, their likelihood can be defined as

$$p(z_i|M) = \eta \exp\left\{-\frac{1}{2}\left(\frac{z_i - d\left(N\big|_M^{z_i}\right)}{\sigma}\right)^2\right\} \tag{9}$$

where M is the map, η is a normalizing term, and σ is the range uncertainty Lee and Chung (2009). Based on (9), the ML grid map is obtained through

$$\begin{aligned}\overline{M} &\equiv \underset{M}{\textbf{argmax}}\ p(Z|M)\\ &= \underset{M}{\textbf{argmax}}\ \prod_i p(z_i|M) &(10)\\ &= \underset{M}{\textbf{argmax}}\ \sum_i \log p(z_i|M) &(11)\\ &= \underset{M}{\textbf{argmin}}\ \sum_i \left(z_i - d\left(N\big|_M^{z_i}\right)\right)^2 &(12)\end{aligned}$$

where $Z = \{z_1, \cdots, z_n\}$. A static world assumption is used in (10), indicating that other sensor measurements are conditionally independent when map M is given (Thrun et al. 2002; Thrun 2003). The log function is introduced for reducing computational costs in (11), and the application of simple algebra results in (12). Eventually, the ML approach becomes a problem to minimize the sum of quadratic functions. The ML approach suffers from three typical problems: over-fitting, heavy computational complexity, and local minima.

- Over-fitting is an intrinsic problem of the ML approach (Bishop 2007). Lee and Chung (2009), it was reported that more than 50 % of the sonar measurements were incorrect in general indoor environments. Thus, the ML grid map will be over-fitted to those incorrect measurements and may contain errors.
- The solution to (12) is to minimize the sum of all quadratic functions, which involves a complexity of $O(2^k n)$ where k is the number of cells in a map and n is the number of sonar readings. The likelihood of all measurements n must be calculated for the 2^k possible maps leading to a complexity of $O(2^k n)$. This high complexity makes the ML approach unsuitable for practical use.
- The expectation-maximization (EM) algorithm (Dempster et al. 1977) can be used to reduce the complexity, but may fall into a local minimum, making determination difficult of whether the solution is a global or simply a local minimum.

5.1.2 Maximum approximated likelihood (MAL) approach

The maximum approximated likelihood (MAL) approach was proposed in Lee and Chung (2009) to resolve the problems inherent in the ML approach. The MAL approach can be summarized by the following:

$$\begin{aligned}\overline{M} &\equiv \underset{M}{\textbf{argmax}}\ p(Z_1|M) &(13)\\ &= \underset{M}{\textbf{argmin}}\ \sum_{z_i \in Z_1} \left(z_i - d\left(N\big|_M^{z_i}\right)\right)^2 &(14)\\ &\simeq \underset{M}{\textbf{argmin}}\ \sum_{z_i \in Z_1} g(z_i) &(15)\end{aligned}$$

where Z_1 is the set of correct measurements and $g(z_i)$ is defined as

$$g(z_i) \equiv \begin{cases} 0 & \text{for} \quad \left|z_i - d\left(N\big|_M^{z_i}\right)\right| \le \beta \\ \left(z_i - d\left(N\big|_M^{z_i}\right)\right)^2 & \text{for} \quad \left|z_i - d\left(N\big|_M^{z_i}\right)\right| > \beta \end{cases}. \tag{16}$$

As proved in Lee and Chung (2009), the ML approach can be converted to a problem of simple logic if the incorrect measurements, which cause conflict cells, are removed. Thus in (13), the MAL approach integrates only correct

measurements into the map, and this is helpful in indirectly avoiding the over-fitting problem of the ML approach.

To reduce the huge complexity, the MAL approach in (15) approximates the minimization of (14) by relaxing the margin $\pm\beta$ for the range uncertainty β shown in Fig. 3. In general, this approximation reduces the complexity slightly. Fundamentally, the assumption that no conflict cells exist among correct measurements converts the high-dimensional optimization in (15) to a simple logic. This assumption drastically reduces the $O(2^k n)$ complexity of the ML approach to $O(n)$, and the globally minimized solution of (15) is achievable.

Although the MAL approach overcomes the problems of the ML approach directly or indirectly, it excludes incorrect measurements from the mapping process. Thus, it can suffer from the same lack of information insufficiency illustrated in Fig. 1.

5.2 Enhanced maximum likelihood (eML) approach

To resolve the problem of insufficient information, the eML approach integrates incorrect measurements into a map instead of removing them. An eML map consists of two sub-maps; one is generated from correct measurements Z_1, and the other is from incorrect measurements $\bar{Z}_2$.

Before proceeding further, we assume that all sonar readings are classified into two groups: correct and incorrect. Details of the classification process are described in Sect. 4. Henceforth, the set of all sonar readings is the sum of two subsets ($Z = \{Z_1, \bar{Z}_2\}$).

5.2.1 Model

Although an incorrect reading fails to provide correct information about the existence of obstacles in its arc region, it is not entirely wrong and part of the reading contains useful information. As illustrated in Fig. 6, the portion of the measurement closest to the sensor contains correct information about the empty region. Thus, if the correct portion is extracted, it can be integrated into a map to compensate for an unrepresented area without degrading the map quality. Thus incorrect measurements $\bar{Z}_2$ can be reprocessed by adjusting

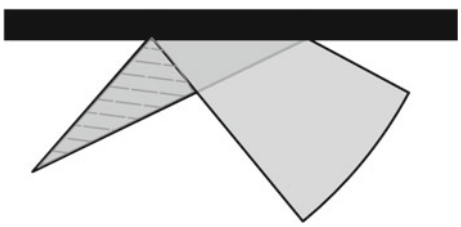

Fig. 6 As shown in the hatched area, an incorrect measurement which fails to detect the closest obstacle contains correct information about the empty region

their range, and reprocessed measurements Z_2 will be used in the mapping.

The eML map is defined as follows:

$$\overline{M} \equiv \underset{M}{\mathbf{argmax}}\ p(Z'|M) \tag{17}$$

$$= \underset{M}{\mathbf{argmin}} \left\{ \sum_{z_i \in Z_1} \left(z_i - d\left(N|_M^{z_i}\right)\right)^2 + \sum_{z_j \in Z_2} \left(z_j - d\left(N|_M^{z_j}\right)\right)^2 \right\} \tag{18}$$

$$\simeq \underset{M}{\mathbf{argmin}} \left\{ \sum_{z_i \in Z_1} g(z_i) + \sum_{z_j \in Z_2} g(z_j) \right\}. \tag{19}$$

Instead of using original incorrect measurements $\bar{Z}_2$ in (17), reprocessed readings Z_2 are used to build an eML map. More specifically, instead of $Z(= \{Z_1, \bar{Z}_2\})$, the new measurements set $Z'(= \{Z_1, Z_2\})$ is used to build the map. (18) is obtained by applying the definition of the likelihood of a sonar reading (9). Finally, approximating the quadratic functions in (18) as was done for (15) results in (19). For the sake of simplicity,

$$h(Z_a, M) \equiv \sum_{z_i \in Z_a} g(z_i)\Big|_M \quad \text{for } a = \{1, 2\}, \tag{20}$$

and (19) becomes

$$\overline{M} \simeq \underset{M}{\mathbf{argmin}} \{h(Z_1, M) + h(Z_2, M)\}. \tag{21}$$

5.2.2 Constraints

To solve (21), we assume two sub-maps that satisfy the following:

$$M_1 = \{M | h(Z_1, M) = 0\} \tag{22}$$

$$M_2 = \{M | h(Z_2, M) = 0\}. \tag{23}$$

Because the functions $h()$ in (22) and (23) consist of quadratic functions, they cannot be less than zero, and zero is the smallest value achievable. Therefore, for each set of measurements, M_1 and M_2 are the globally minimum solution of each $h()$. If M_1 and M_2 exist as we have assumed, then (21) can be converted to

$$\overline{M} \simeq \underset{M}{\mathbf{argmin}}\ h(Z_1, M) \cup \underset{M}{\mathbf{argmin}}\ h(Z_2, M) \tag{24}$$

$$= M_1 \cup M_2. \tag{25}$$

In (25), $\overline{M}$ is represented by the sum of M_1 and M_2. Completing this representation, however, requires determining whether M_1 and M_2 are coupled. Thus, the following constraints should be satisfied to make the sub-mapping in (25) perfect:

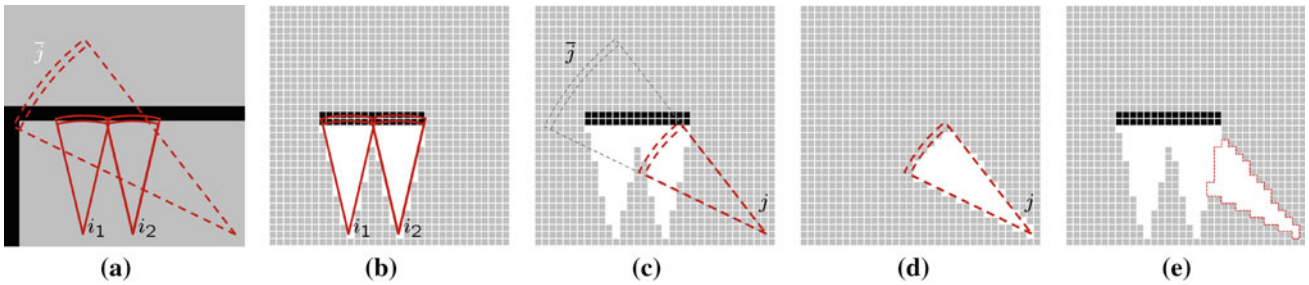

Fig. 7 Example of the eML approach. **a** The case of three sonar measurements where measurements i_1 and i_2 are correct, and measurement $\bar{j}$ is determined to be incorrect. The decision process is described in Sect. 4. **b** Based on correct measurements i_1 and i_2, M_1 is built by the MAL approach. **c** Based on M_1, the incorrect measurement $\bar{j}$ is reprocessed and becomes new measurement j. **d** M_2 is generated using M_1 and j. **e** The eML map is produced by merging M_1 and M_2. The *dotted area* indicates the additional region obtained by reprocessing the incorrect measurement

$$h(Z_1, \overline{M}) = h(Z_1, M_1) \tag{26}$$

$$h(Z_2, \overline{M}) = h(Z_2, M_2). \tag{27}$$

(26) ensures that M_2 does not affect $h(Z_1, M_1)$, and (27) ensures that M_1 does not increase or decrease $h(Z_2, M_2)$.

In summary, the final solution $\overline{M}$ is represented by the sum of two sub-maps M_1 and M_2. Four constraints (22), (23), (26), and (27) must be satisfied to achieve the sub-map representation.

5.2.3 Solution

To this point, we have not described how to determine the reprocessed measurements Z_2. Thus, M_2, in (23), cannot be calculated. Unlike M_2, M_1 is fixed due to the fixed Z_1 and can be readily generated. This is consistent with the physical perspective that map M_1, built by correct measurements Z_1, should not be changed by incorrect readings.

- M_1 : M_1 is obtained by the MAL approach (Lee and Chung 2009) although there is one precondition for doing so. The precondition is that all correct measurements Z_1 should not cause conflict cells. Fortunately, the measurements determined correct by the mSP method satisfy the condition, as shown in the Appendix A. Given three sonar readings ($i_1, i_2 \in Z_1$ and $j \in \bar{Z}_2$) as shown in Fig. 7a, M_1 is generated with i_1 and i_2 using the MAL approach because they are correct readings (Fig. 7b).
- Z_2 : Based on M_1, the original incorrect measurements $\bar{Z}_2$ can be reprocessed into new measurements Z_2 by

$$Z_2 = \left\{ z_j \middle| z_j = d\left(N\big|_{M_1}^{\bar{z}_j}\right) \right\} \text{ for } \bar{z}_j \in \bar{Z}_2 \tag{28}$$

where z_j is the new range of the reprocessed measurement. (28) means that the range of new reprocessed measurements is determined by the distance to the closest occupied cell within the beamwidth of an original incorrect measurement on map M_1. For example, as illustrated in Fig. 7(c), the range of the incorrect measurement $\bar{j}$ reduced to the nearest occupied cell in M_1, and the incorrect measurement $\bar{j}$ becomes j.

- M_2 : Once Z_2 has been determined, M_2 can be generated by

$$M_2 = \left\{ M \middle| O_c(M) = \bigcup_{\bar{z}_j \in \bar{Z}_2} N\big|_{M_1}^{\bar{z}_j} \right.$$
$$\left. \text{and } E_c(M) = \bigcup_{z_j \in Z_2} F(z_j) \right\} \tag{29}$$

where $O_c(M)$ and $E_c(M)$ are all occupied cells and all empty cells in M, respectively. The $N\big|_{M_1}^{\bar{z}_j}$s are found while calculating Z_2 in (28), and then only $N\big|_{M_1}^{\bar{z}_j}$s are marked as occupied in M_2. Additionally, the cells of the free region of the reprocessed measurements $F(z_j)$ are marked as empty in M_2. As illustrated in Fig. 7d, all occupied cells in M_2 are the same as $N\big|_{M_1}^{\bar{z}_j}$, and all empty cells make up the free region of new measurements Z_2.

$\overline{M}$ is determined by merging M_1 with M_2, as shown in Fig. 7e where the dotted area indicates the additional region obtained using incorrect measurements appropriately. The details about satisfying four constraints (22), (23), (26), and (27) are as follows:

- (22): Lee and Chung (2009) proved that M_1 satisfies (22).
- (23): While building M_2, the occupied cells are acquired from $N\big|_{M_1}^{\bar{z}_j}$ and the distance to $N\big|_{M_1}^{\bar{z}_j}$ determines the range of new measurement Z_2. Therefore, $z_j - d\left(N\big|_{M_1}^{\bar{z}_j}\right) = 0$ for $z_j \in Z_2$. Eventually, this brings all quadratic functions of $h(Z_2, M_2)$ to zero, and thus the second constraint (23) is satisfied.

– (26): All occupied cells of M_2 is obtained from M_1 as provided in (29), i.e., $O_c(M_2) = \left(\bigcup_{\bar{z}_j \in \bar{Z}_2} N\big|_{M_1}^{\bar{z}_j} \right) \in O_c(M_1)$. Thus, M_2 does not affect $h(Z_1, M_1)$, and (26) is satisfied.
– (27): As in (29), $O_c(M_2)$ is generated from the nearest occupied cell within the beamwidth of an original incorrect measurement on the map M_1, so that $h(Z_2, M_2) = h(Z_2, M_1)$. Thus, $h(Z_2, M_1 \cup M_2) = h(Z_2, M_2)$. The same applies to (27).

Because M_1 and M_2 minimize each $h()$ as shown in (22) and (23), respectively, $\overline{M}(= M_1 \cup M_2)$ becomes the solution that globally maximizes the likelihood of sonar measurements, as shown in (21). The complexity of the eML approach is $O(n)$; $O(n)$ to build M_1 (Lee and Chung 2009), $O(n)$ to acquire new measurements Z_2, and $O(n)$ to build M_2.

6 Method overall

Integrating the eML approach with the mSP method results in the Maximum Likelihood based on Sub-maps (MLS) approach outlined in Algorithm 1. After collecting sonar readings, the mSP method determines the status of each measurement (line 1–2 in Algorithm 1), and then the eML approach builds a map with all measurements based on their status (line 3–6 in Algorithm 1). The complexity of the MLS approach is $O(n)$: $O(n)$ for the mSP method and $O(n)$ for the eML approach.

Algorithm 1 The MLS approach

Require: All sonar measurements (Z)

1: $\widehat{M} \leftarrow$ build the mSP map by Eq. (7) and (8)
2: $Z = \{Z_1, \bar{Z}_2\} \leftarrow$ classify all measurements into two categories using $\widehat{M}$ by Eq. (1)
3: $M_1 \leftarrow$ build a map using all correct measurements Z_1 by the MAL approach (Lee and Chung 2009)
4: $Z_2 \leftarrow$ reprocess the range of all incorrect measurements $\bar{Z}_2$ using M_1 by Eq. (28)
5: $M_2 \leftarrow$ build a map using all reprocessed measurements Z_2 by Eq. (29)
6: $M \leftarrow$ build the eML map using M_1 and M_2 by Eq. (25)

7 Experimental results

7.1 Experimental setup

To test the performance of the MLS approach, we conducted experiments in several indoor environments using two types of well-known sonar sensors: S600 and MA40B8. Figure 8 shows the configurations of these sensors. The experimental environments were grouped into corridor environments designated C#1 and C#2, home-like environments designated H#1-5, and unstructured environment designated U#1. The experiment with the MA40B8 were conducted in all environments, while the S600 was used only in C#1, C#2, H#1, and U#1. Only two results for the MA40B8 and the S600 are illustrated in this paper due to space limitations, while the other results are summarized in tables, on graphs, or in the provided supplementary materials. In particular, because the performance of the MLS approach was significant when there were insufficient measurements, such as in the case of using only two sonar sensors, the two-sensor case is described in detail and the others are included in the supplementary materials. The details of the experimental specifications are as follows:

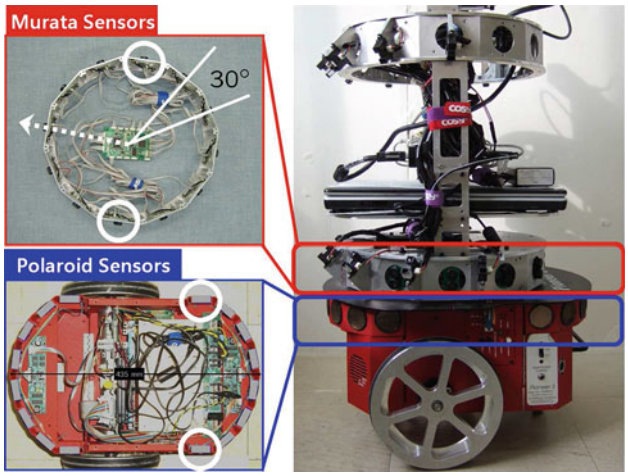

Fig. 8 Configuration of the sonar sensors used in the experiments. The *upper-left image* shows 12 MA40B8 sensors and the white *dotted arrow* indicates the direction of robot travel. In the *lower-left figure*, each *gray box* represents the position of one of the 16 S600 sensors. The *white circles* indicate the two sonar sensors used in the experiments for insufficient measurements

– Map
  – Cell size: 5 cm ×5 cm
– Measurement
  – Maximum admissible range: 4 m[1]
  – Sampling frequency: 4 Hz
– Motion: Manual movement
  – Translational velocity: 150 mm/s
  – Rotational velocity: 25°/s

[1] Because the divergence between the theoretical and the measured beamwidth starts to increase rapidly around 4m according to Burguera (2009b) and our experiences, the maximum admissible range was limited to 4m.

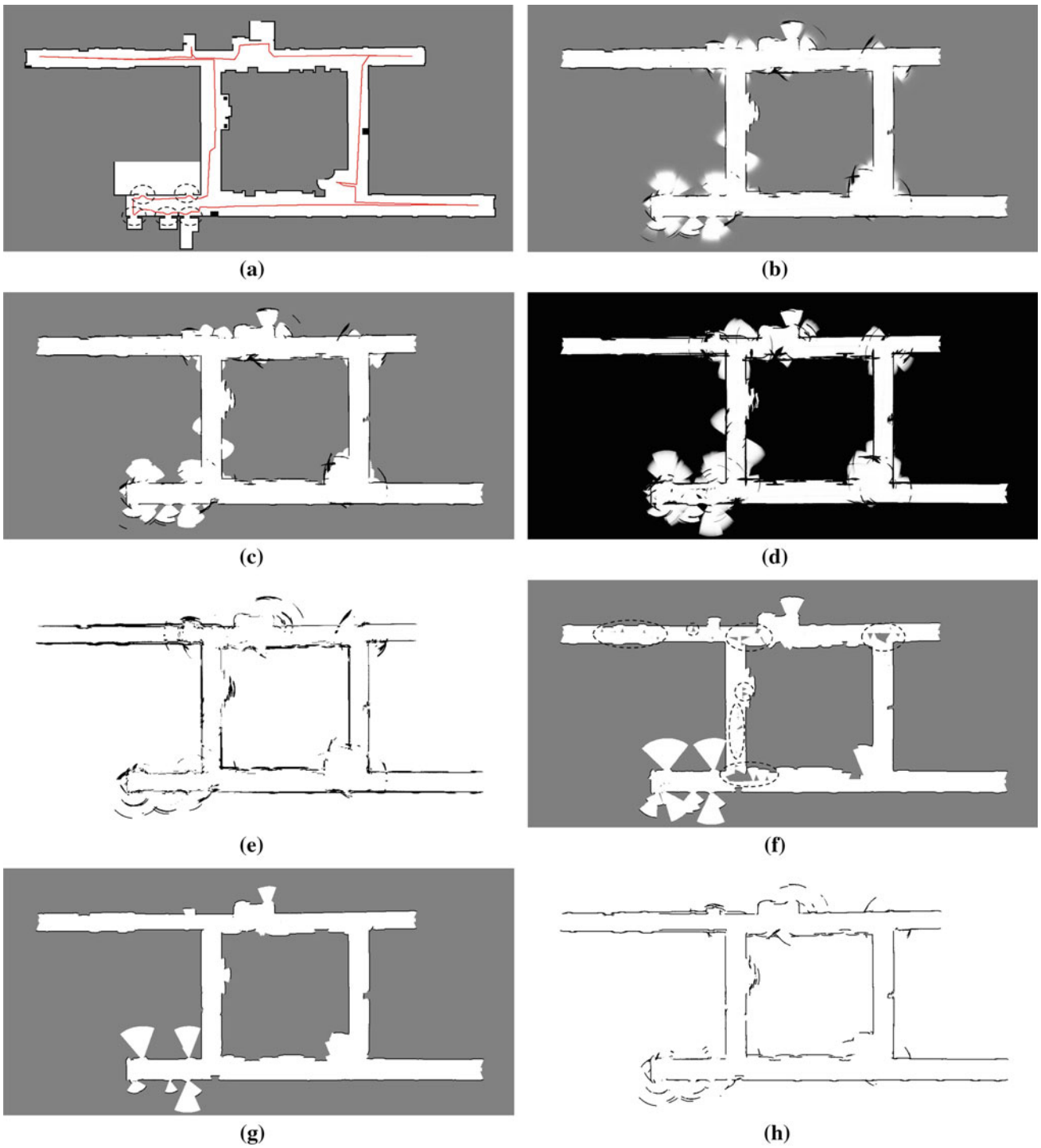

Fig. 9 Experimental results in environment C#1 (62 m × 30 m) with only two MA40B8 sensors: **a** Reference map. The *line* indicates the trajectory of the robot, and the *dashed areas* represent narrow openings. **b** PT map. **c** DS map. **d** FZ map. The FZ map originally sets the state of a cell to safe (*white*) or unsafe (*black*). **e** ML map. The ML map contains only occupied and empty cells because the ML approach originally sets the state of a cell to occupied (*black*) or empty (*white*). **f** CEMAL map. The *dashed areas* are unrepresented regions. **g** Our approach: MLS map. **h** Our approach: mSP map

7.2 Mapping performance

We compared the performance of the MLS approach with a number of representative grid mapping approaches: the posterior approach (PT), the Dempster–Shafer approach (DS), the fuzzy approach (FZ), the maximum likelihood approach (ML), and the conflict evaluated maximum approximated likelihood approach (CEMAL). As described in

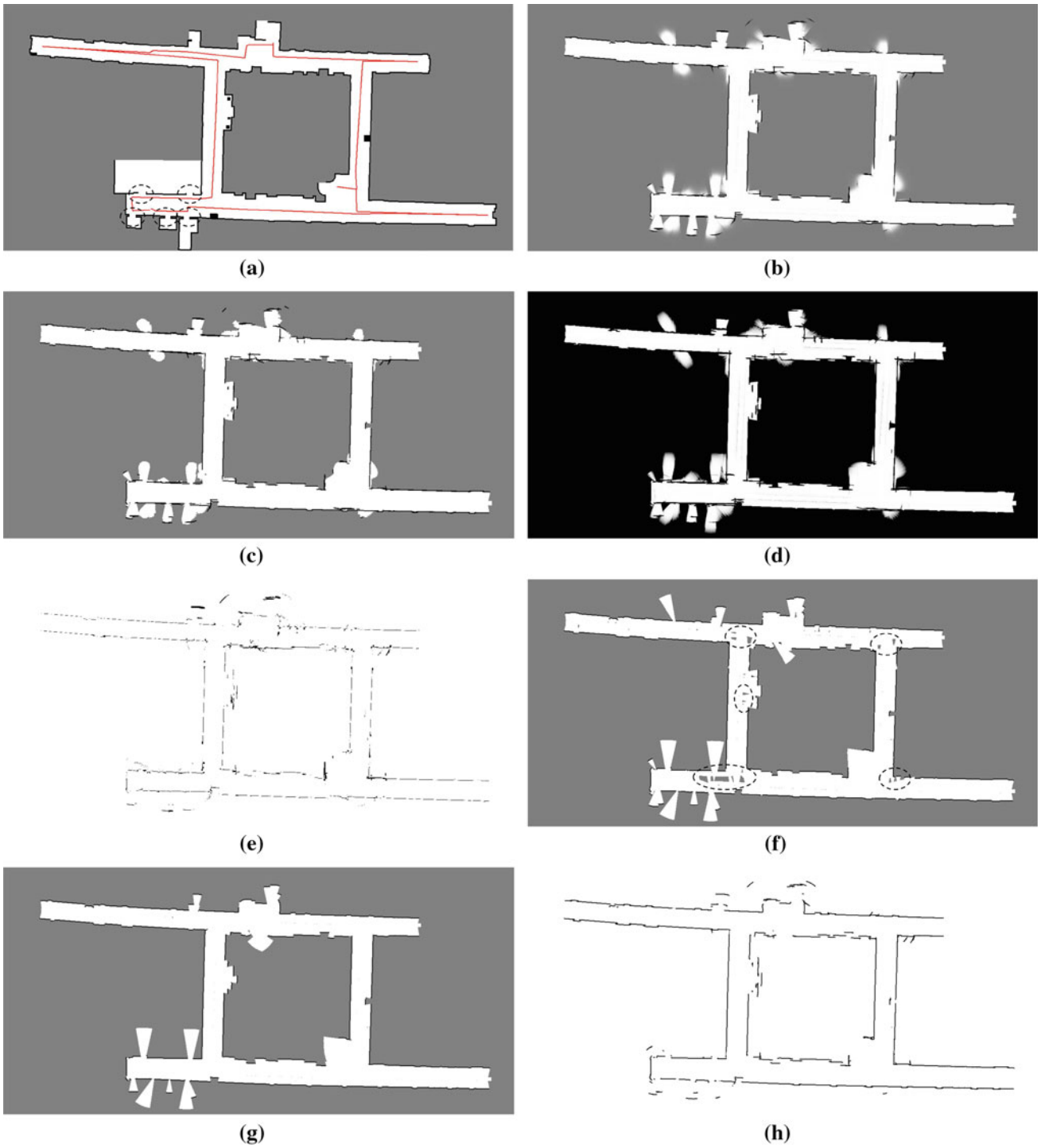

Fig. 10 Experimental results in environment C#1 (62 m × 30 m) with only two S600 sensors: **a** Reference map. The *line* indicates the trajectory of the robot, and the *dashed areas* represent narrow openings. **b** PT map. **c** DS map. **d** FZ map. **e** ML map. **f** CEMAL map. The *dashed areas* are unrepresented regions. **g** Our approach: MLS map. **h** Our approach: mSP map

Lee and Chung (2009), PT, DS, and FZ require adjustment of the update parameters. For these approaches, the parameter set that minimized the wrong cell ratio (WCR, described below) was used to build the grid maps. The EM algorithm Dempster et al. (1977) was used with ML to reduce the computational burden.

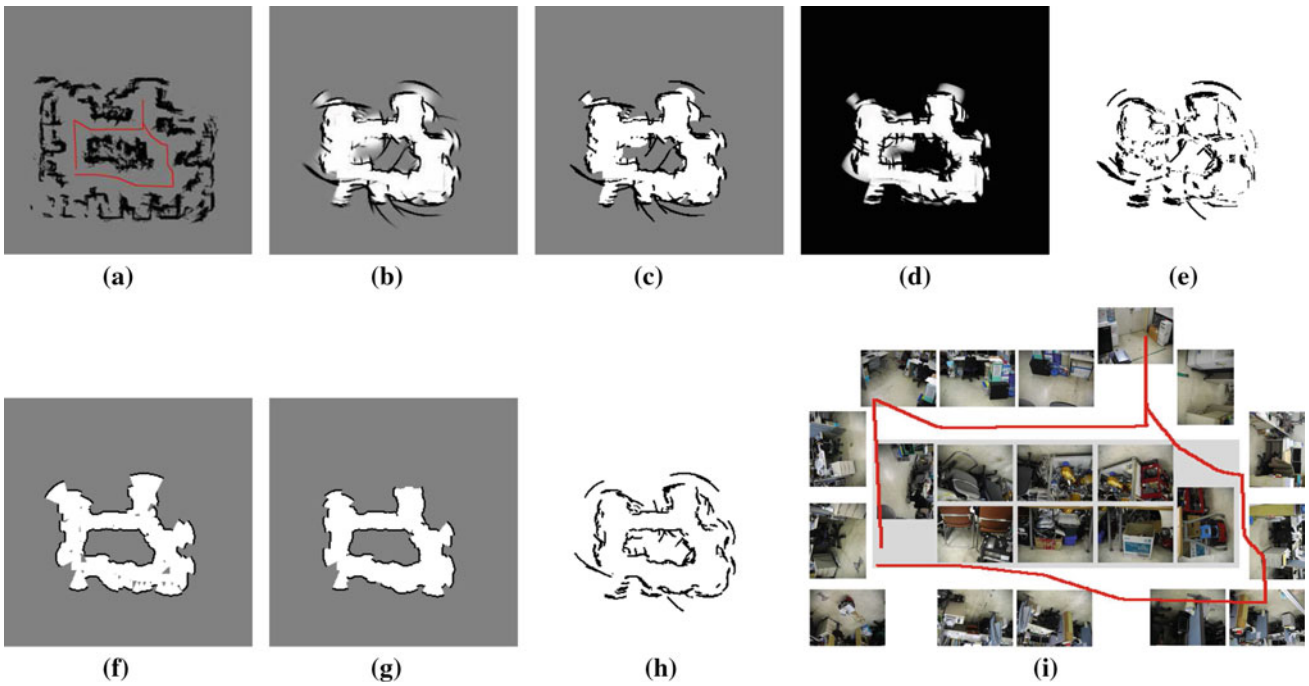

Fig. 11 Experimental results in environment U#1 (14 m × 14 m) with only two MA40B8 sensors: **a** Reference Map. The line indicates the trajectory of the robot, and is the same with the line in (i). **b** PT map. **c** DS map. **d** FZ map. **e** ML map. **f** CEMAL map. **g** Our approach: MLS map. **h** Our approach: mSP map. **i** Snapshots in unstructured environment. The *line* indicates the trajectory of the robot

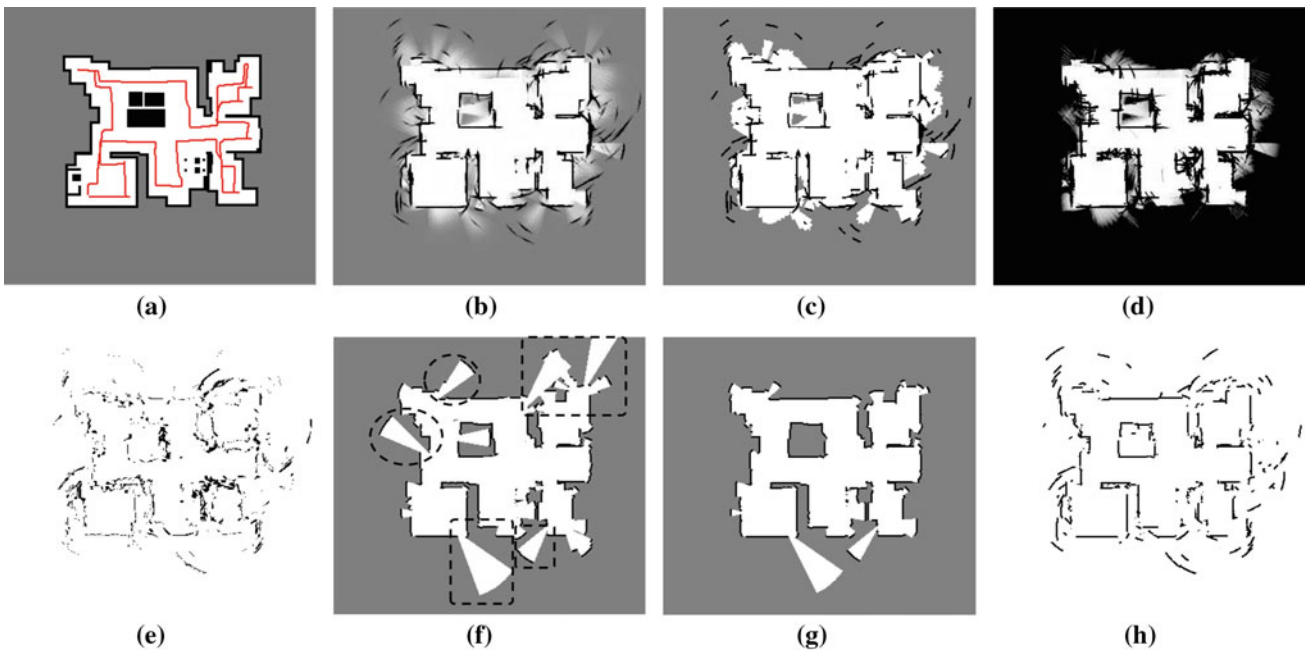

Fig. 12 Experimental results in environment H#1 (18 m × 16 m) with only two S600 sensors: **a** Reference map. The *line* indicates the trajectory of the robot. **b** PT map. **c** DS map. **d** FZ map. **e** ML map. **f** CEMAL map. The *dashed areas* indicate regions of significant error caused by wrong decisions about incorrect measurements. **g** Our approach: MLS map. **h** Our approach: mSP map

7.2.1 Qualitative comparison

Accurate reference maps are necessary to evaluate the quality of a map. We used data from a laser range finder (LRF) as well as a blueprint of each environment to build the reference maps. The blueprints make up for obstacles that the LRF sometimes misses, and the LRF provides detailed information that the blueprint does not contain. In detail, after

building a LRF-based grid map, a reference map is obtained by combining the grid map with the blueprint. Figures 9, 10, 11, 12a show the reference maps.

Figures 9, 10, 11, 12b–d show the results of the independent estimation approaches PT, DS, and FZ. Although the overall shape of each environment was captured successfully, the maps still include errors where areas behind the wall of the environment were expressed as empty. The errors were the result of improper handling of the angular uncertainty and the effect of incorrect measurements as described in Sect. 2. If the parameters of each approach are modified to show occupied regions, this causes previously unrepresented obstacles to be shown, but also results in the appearance of ghost obstacles. Conversely, if the parameters are adjusted in the opposite direction, ghost obstacles disappear, but so do some real obstacles. Thus, adjusting the parameters for each of these approaches is difficult.

On the other hand, as shown in Figs. 9, 10, 11, 12e, the results of the ML approach successfully represented the overall shape of the environment as well as the inner area without any parameter adjustments, although erroneous parts in the outside area remained. Specifically, in terms of representing narrow openings, the maps in Figs. 9e and 10e are not satisfactory because incorrect measurements obstructed a clear representation.

Figures 9, 10, 11, 12f, which are the results of the CEMAL approach, are good, compared with the other results. The CEMAL approach faithfully represented the overall shape of the environment and indicated occupied regions accurately. It did, however, omit some empty areas in the inner region of the environment because incorrect sonar measurements were excluded from the mapping and the exclusion caused insufficient measurement to cover the whole environment. Additionally, wrong decisions about incorrect measurements cause errors as shown in Fig. 12f. In other environments, as shown in the supplementary materials, results of the CEMAL approach were similar to Figs. 9, 10, 11, 12f in terms of overall representation, partial omission, and errors from wrong decisions.

In contrast, the result of the MLS approach (Figs. 9, 10, 11, 12g) are excellent in terms of map quality; the occupied regions are shown more accurately and the empty regions are placed more clearly, compared with the other results. The narrow openings in particular are clearly represented. Furthermore, the MLS approach successfully showed areas not represented by the CEMAL approach, and reduced the extent of some erroneous parts that the CEMAL approach failed to represent correctly.

7.2.2 *Quantitative comparison*

We defined a criterion for quantitatively evaluating and comparing the performance of the mapping approaches. This

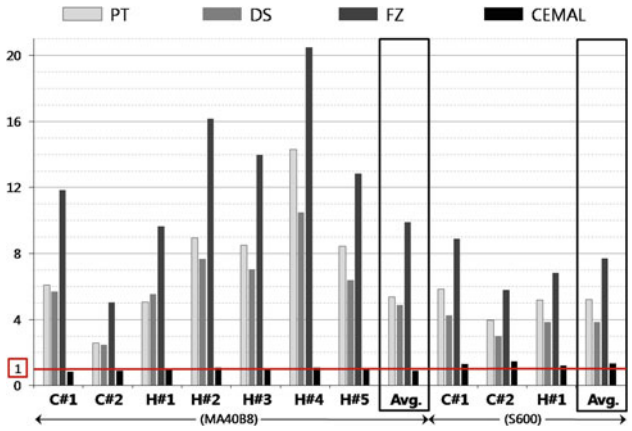

Fig. 13 Wrong cell ratios (WCR) for the different approaches when using all sonar sensors. One experiment was conducted for each environment. The case for U#1 is omitted because that environment was very cluttered and the laser sensor alone was incapable of providing an exact reference map

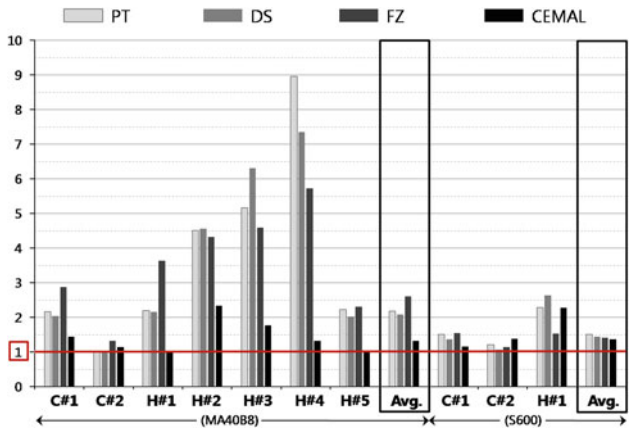

Fig. 14 Wrong cell ratios (WCR) for the different approaches when using only two sonar sensors. One experiment was conducted for each environment

is the wrong cells ratio (WCR) that indicates how much of the map contains wrong regions. The WCR is given by

$$\mathrm{WCR} = \frac{\#\text{of wrong cells in the map being evaluated}}{\#\text{of wrong cells in the MLS map}} \quad (30)$$

where a wrong cell is a cell that has a different state than in the reference map. The WCR is a relative error measure with respect to the error of the MLS map. Thus, when the WCR is greater than 1, the map being evaluated has more errors than the MLS map.

Figure 13 shows that the MLS approach had performance superior to that of PT, DS, and FZ, and was similar to the CEMAL approach in terms of WCR when using all sonar sensors. Figure 14 indicates that the MLS approach had the best performance in terms of WCR when using only two sonar sensors. The WCR results indicated that a MLS map contains the smallest number of wrongly represented cells.

Table 2 Total computational time (*s*)

	Env.	Size of env.	# of measurements		PT		DS		FZ		ML		CEMAL		MLS	
MA40B8	C#1	62 m×32 m	75,720	(12,620)	37	(2.5)	38	(2.6)	75	(5.1)	47,500	(808.6)	105	(8.0)	91	(7.5)
	C#2	50 m×15 m	20,808	(3,468)	9	(0.5)	9	(0.6)	18	(1.0)	11,596	(82.1)	19	(1.5)	23	(1.7)
	H#1	18 m×16 m	33,864	(5,644)	10	(0.9)	10	(1.0)	22	(2.0)	26,071	(1307.1)	38	(3.4)	26	(3.1)
	H#2	20 m×20 m	17,100	(2,850)	6	(0.7)	6	(0.6)	13	(1.2)	7,346	(687.7)	12	(1.8)	14	(1.8)
	H#3	15 m×15 m	17,856	(2,976)	4	(0.4)	4	(0.4)	8	(0.8)	9,807	(591.1)	19	(1.3)	10	(1.2)
	H#4	15 m×16 m	33,360	(5,560)	7	(0.9)	8	(0.9)	17	(1.7)	14,293	(973.3)	34	(2.9)	20	(2.5)
	H#5	15 m× 15 m	26,196	(4,366)	5	(0.4)	5	(0.4)	12	(1.1)	11,506	(621.2)	22	(1.4)	15	(1.4)
	U#1	14m×14 m	8,472	(1,412)	1	(0.1)	1	(0.1)	3	(0.2)	3,859	(99.6)	3	(0.2)	2	(0.2)
	Avg.		233,376	(38,908)	10	(0.8)	10	(0.8)	21	(1.6)	16,497	(646.3)	32	(2.5)	25	(2.4)
S600	C#1	62 m×32 m	97,504	(12,188)	41	(1.4)	42	(1.5)	72	(2.7)	4,297	(86.2)	81	(2.2)	106	(4.1)
	C#2	50 m×15 m	29,296	(3.662)	11	(0.4)	11	(0.4)	20	(0.8)	1,258	(30.5)	21	(0.7)	29	(1.3)
	H#1	18 m×16 m	51,504	(6,438)	15	(1.0)	15	(1.0)	28	(1.7)	7,239	(152.7)	43	(1.6)	43	(2.7)
	U#1	14 m×14 m	12,592	(1,574)	3	(0.1)	3	(0.1)	5	(0.3)	1,135	(18.1)	4	(0.3)	7	(0.6)
	Avg.		190,896	(23,864)	17	(0.7)	18	(0.8)	31	(1.4)	3,482	(71.9)	37	(1.2)	46	(2.1)

The value in parenthesis indicates the case of using only two sonar sensors, and the other is for using the complete band of sonar sensors (OS: Windows XP, CPU: 2.6-GHz Pentium 4, Language: C++, Application: Single thread application)

Table 3 Summary of mapping approaches

	Complexity	Dominant memory usage [a]	Processing	Empirical[b] error
PT	$O(n)$	n	Online	5.1 (1.8)
DS	$O(n)$	n	Online	4.2 (1.7)
FZ	$O(n)$	n	Online	8.8 (2.1)
ML	$O(2^k n)$	$\gg n$	Offline	N/A[c]
CEMAL	$O(n^2)$	$\gg n$	Online	1.2 (1.4)
MLS	$O(n)$	n	Offline	1 (1)

[a]The dominant memory usage excludes memory required to store the map
[b]This error is the wrong cell ratio (WCR), and the value in parentheses indicates the case of using only two sonar sensors
[c]Because the ML approach originally sets the state of a cell to occupied or empty, the WCR cannot be measured

7.2.3 Computational load

Table 2 shows the total computation time required to create the map using each approach. The ML computation required a very long time compared to the other approaches despite using the EM algorithm. On the other hand, while the MLS approach is based on the ML approach, its execution time was comparable to the other estimation approaches. The MLS time was somewhat longer because the MLS is a two-layered approach incorporating a filtering layer (mSP) and a fusion layer (eML), while PT, DS, and FZ, have only a fusion layer. Although it was longer, the MLS execution time was not prohibitive for practical use.

7.2.4 Overall comparison

Table 3 summarizes properties of mapping approaches. Except the ML approach and the CEMAL approach, all mapping approaches have the complexity of $O(n)$ where n is the number of measurements. In terms of memory usage, the ML approach and the CEMAL approach use the most. Empirically, they require approximately 600 times the memory compared to the MLS approach. This is because both ML and CEMAL store indices or pointers of all related measurements in each cell in order to decrease the search time. Except the ML approach and the MLS approach, all mapping approaches can build a map incrementally. Through several indoor experiments, quality of MLS map is shown the best not only in the case of using the complete band of sonar sensors but also in the case of using only two sonar sensors.

7.3 Decision performance

In Sect. 2, we described the result of research into the rejection of incorrect sonar measurements. We selected representative methods RCD, spAC, RANSAC/GF, NVD, NN, and CEsp to compare with the mSP method.

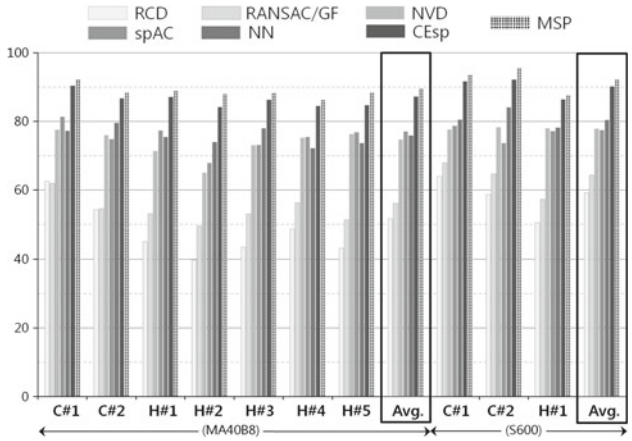

Fig. 15 Correct decision ratio (CDR) for the different approaches when using all sonar sensors

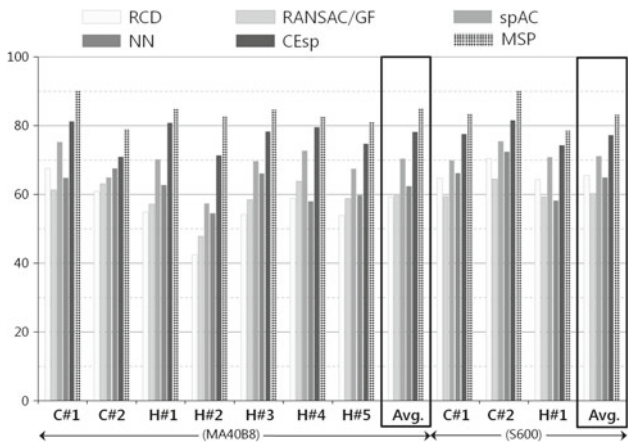

Fig. 16 Correct decision ratio (CDR) for the different approaches when using only two sonar sensors. The result of the NVD method is not included because it cannot be used with only two sensors

The correct decision ratio (CDR) from Lee and Chung (2009) was used for the purposes of quantitative comparison. The CDR indicates the proportion of measurements correctly determined through a filtering process. Thus, higher values

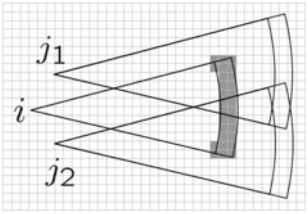

Fig. 17 Shaded *gray cells* indicate conflict cells. If the three measurements are correct, conflict cells should not occur. Thus, the incorrect measurements should be included in this case

of CDR indicate better decision performance to a maximum of 100.

As shown in Figs. 15 and 16, the mSP method had the best performance for correctly determining the state of measurements, with a CDR of about 91 % when using all sonar sensors and about 84 % when using only two sonar sensors.

8 Conclusion

A small number of sonar sensors is desirable to reduce cost and processing resources. Thus, we began this research by asking how to build an accurate grid map, using a small number of error-prone sonar sensors. Empirically, when there are insufficient sonar measurements, the grid map frequently misrepresents some empty regions because correct sonar measurements cannot cover the whole area. If incorrect measurements are used without appropriate processing to recover unrepresented regions, they will degrade the quality of the map. To address this issue, we started with the ML approach because of its suitability for handling inconsistent information, as described in Sect. 2. The ML approach, however, has three critical problems: over-fitting, heavy computational complexity, and local solutions. These problems degrade the quality of the ML map, and prevent its use in practical applications. Thus, obtaining a high-quality grid map requires simultaneously incorporating incorrect measurements appropriately and overcoming the problems of the ML approach.

To achieve that, we proposed the MLS approach, which consists of two layers: the decision layer (the mSP method) and the mapping layer (the eML approach). The mSP method determines if sonar readings are incorrect or correct based on the extended application of sound pressure. Because measurements determined to be correct do not cause conflict cells, they can be used to build the eML map. The eML approach builds two sub-maps; one is based on correct measurements and the other is from incorrect measurements. The eML map is obtained by merging these two maps. In other words, the eML approach is a type of divide-and-conquer algorithm.

To our knowledge, the MLS approach is the only mapping methodology that integrates incorrect measurements into a map in a well-defined manner. The MLS approach can generate an accurate and precise map even with only two error-prone sonar sensors by the appropriate handling of incorrect measurements. This indicates that the MLS approach is less sensitive to the number of sonar sensors when building a high-quality grid map than previous mapping approaches. Although the MLS approach is based on the ML approach, its complexity is $O(n)$, which is very low compared to the $O(2^k n)$ of the ML approach. Moreover, the MLS map succeeds in globally maximizing the likelihood of sonar measurements with a divide-and-conquer approach. Additionally, the mSP method is better than existing methods at determining the true state of sonar measurements in the case when a complete band of sensors is used or when only two sonar sensors are used. Several indoor experiments confirmed that the MLS approach was a good mapping methodology in terms of the quality of the map, the low algorithm complexity, and the ability to build map with a small number of sonar sensors.

There are three significant aspects of the MLS approach. First, while conducting our experiments, the robot followed the corridors or the walls, and its two sonar sensors had been on the right and left sides of the robot (Fig. 8) to reduce the proportion of incorrect measurements. If these two sensors were on the front and rear of the robot, almost all sonar measurements would have been incorrect due to the undesirable reflections that would result from such a geometry. When almost all measurments are incorrect, the mSP method and the MLS approach do not produce usable results because proper information is seriously sparse to model the environment. Thus, when only two sonar sensors are used to build a grid map, their configuration may be critical to obtain useful measurements. Second, all experiments were conducted in a static environment. Third, we assumed that pose estimations were available because localization during mapping was not a concern in this study. The pose estimations rely on EKF-SLAM [extended Kalman filter-simultaneous localization and mapping) (Ahn et al. (2008)]. The quality of the MLS grid map cannot be guaranteed if the level of pose estimation error is excessive. In our experiments, the maximum error between the real final pose and the estimated final pose was approximately 10 cm in both the x and y directions.

Acknowledgments The authors would like to the anonymous reviewers for their valuable suggestions for improving the manuscript

Proof of condition for the MSP method

As described in Sect. 5, the measurements regarded as correct should not cause conflict cells if the eML approach is to be used. This can be proved by the following theorem.

Theorem 1 *The mSP method, i.e., the decision based on the mSP map and (1), does not cause conflict cells.*

Proof Let us assume that three measurements i, j_1, and j_2 are classified as correct readings by the mSP method. Additionally, let us assume that these measurements cause conflict cells. Without any loss of generality, we assume that conflict cells occur with the sonar reading i and the other readings j_1 and j_2. As shown in Fig. 17, the whole arc region $A(z_i)$ of the measurement i overlaps free regions $F(j_1)$ and $F(j_2)$.

In this case, by the definition of the correct measurement in (1), the measurement i should contain occupied cells in its arc region. However, if at least one occupied cell exists in the arc region $A(z_i)$, then one or both of the other measurements j_1 and j_2 should be incorrect due to the definition of the incorrect measurement in (1). Conversely, if there are no occupied cells in the arc region $A(z_i)$, then the sonar reading i should be incorrect, because it satisfies the definitions of the incorrect measurement.

As a results, if conflict cells occur, incorrect measurements defined by (1) always exist. Specifically, if conflict cells exist, the first assumption that only correct measurements remain through the mSP method is violated. Therefore, the measurements determined to be correct through the mSP method do not cause conflict cells. □

With Theorem 1, we can confirm that the mSP method can be applied so the eML approach can be used because it does not cause conflict cells. However, Theorem 1 does not apply only to the mSP map. The decision based on a map and (1) does not cause conflict cells for any fixed map. The key property that the map should have is that it is a reasonable representation of the inner region of an environment. If not, the performance of the decision based on the map cannot be guaranteed.

References

Ahn, S., Choi, J., Doh, N. L., & Chung, W. K. (2008). A practical approach for ekf-slam in an indoor environment: Fusing ultrasonic sensors and stereo camera. *Autonomous Robots*, *24*(3), 315–335.

Barshan, B. (2007). Directional processing of ultrasonic arc maps and its comparison with existing techniques. *International Journal of Robotics Research*, *26*(8), 797–820.

Bishop, C. M. (2007). *Pattern recognition and machine learning*. Berlin: Springer.

Burguera, A., Gonzalez, Y., & Oliver, G. (2007). *Probabilistic sonar filtering in scan matching localization* (pp. 4158–4163). In: Proceedings of the IEEE/RSJ international Conference on intelligent robotics and systems.

Burguera, A., Gonzalez, Y., & Oliver, G. (2008). *Sonar scan matching by filtering scans using grids of normal distributions* (pp. 64–73). In: International Conference on intelligent autonomous systems.

Burguera, A., Gonzalez, Y., & Oliver, G. (2009a). On the use of likelihood fields to perform sonar scan matching localization. *Autonomous Robots*, *26*, 203–222.

Burguera, A., Gonzalez, Y., & Oliver, G. (2009b). Sonar sensor models and their application to mobile robot localization. *Sensors (MDPI)*, *9*(12), 10217–10243.

Carlson, J., Murphy, R. R., Christopher, S., & Casper, J. (2005). *Conflict metric as a measure of sensing quality* (pp. 2032–2039). In: Proceedings of the IEEE international conference on robotics and automation.

Choi, J., Choi, M., Nam, S. Y., & Chung, W. K. (2011). Autonomous topological modeling of a home environment and topological localization using a sonar grid map. *Autonomous Robots*, *30*, 351–368.

Choset, H., Nagatani, K., & Lazar, N. (2003). The arc-transversal median algorithm: A geometric approach to increasing ultrasonic sensor azimuth accuracy. *IEEE Transactions on Robotics and Automation*, *19*(3), 513–521.

Dempster, A. P., Laird, N. M., & Rubin, D. B. (1977). Maximum likelihood from incomplete data via em algorithm. *Journal of the Royal Statistical Society Series B (Methodological)*, *39*(1), 1–38.

Fischler, M. A., & Bolles, R. C. (1981). Random sample consensus: A paradigm for model fitting with application to image analysis and automated cartography. *Communications of the ACM*, *24*(6), 381–395.

Hebert, M. (2000). *Active and passive range sensing for robotics* (pp. 102–110). In: Proceedings of the IEEE international conference on robotics and automation.

Ivanjko, E., Petrovic, I., Macek, K., & (2003) Improvements of occupancy grid maps by sonar data corrections. In: Proceedings of FIRA Robot Soccer world congress. Vienna: Austria.

Kleeman, L., & Kuc, R. (2008). Sonar sensing. In O. Khatib & B. Siciliano (Eds.), *Handbook of robotics*. Berlin: Springer.

Kuc, R., & Siegel, M. (1987). Physically-based simulation model for acoustic sensor robot navigation. *IEEE Transactions on Pattern Analysis and Machine Intelligence*, *9*(6), 766–778.

Lee, J. S., & Chung, W. K. (2010). Robust mobile robot localization in highly non-static environments. *Autonomous Robots*, *29*, 1–16.

Lee, K., & Chung, W. K. (2007). *Navigable voronoi diagram: a local path planner for mobile robots using sonar sensors* (pp. 2813–2818). In: Proceedings of the IEEE/RSJ international conference on intelligent robotics and systems.

Lee, K., & Chung, W. K. (2009). Effective maximum likelihood grid map with conflict evaluation filter using sonar sensors. *IEEE Transactions on Robotics*, *25*(4), 887–901.

Leonard, J. J., & Durrant-Whyte, H. F. (1992). *Directed sonar sensing for mobile robot navigation*. Boston: Kluwer Academic.

Moravec, H. P. (1988). Sensor fusion in certainty grids for mobile robots. *AI Magazine*, *9*(2), 61–74.

Murphy, R. R. (1998). Dempster-shafer theory for sensor fusion in autonomous mobile robots. *IEEE Transactions on Robotics and Automation*, *14*(2), 197–206.

Noykov, S., & Roumenin, C. (2007). Occupancy grids building by sonar and mobile robot. *Robotics and Autonomous Systems*, *55*(2), 162–175.

Oriolo, G., Ulivi, G., & Vendittelli, M. (1997). Fuzzy maps: A new tool for mobile robot perception and planning. *Journal of Robotic Systems*, *14*(3), 179–197.

Oriolo, G., Ulivi, G., & Vendittelli, M. (1998). Real-time map building and navigation for autonomous robots in unknown environments. *IEEE Transactions on Systems Man and Cybernetics Part B Cybernetics*, *28*(3), 316–333.

O'Sullivan, S., Collins, J. J., Mansfield, M., Haskett, D., & Eaton, M. (2004). *Linear feature prediction for confidence estimation of sonar readings in map building*. In: Proceedings of the international symposium on artificial life and robotics.

Pagac, D., Nebot, E. M., & Durrant-Whyte, H. F. (1998). An evidential approach to map-building for autonomous vehicles. *IEEE Transactions on Robotics and Automation*, *14*(2), 623–629.

Pathak, K., Birk, A., Poppinga, J., & Schwertfeger, S. (2007). *3d forward sensor modeling and application to occupancy grid based sensor fusion* (pp. 2059–2064). In: Proceedings of the IEEE/RSJ international conference on intelligent robotics and systems.

Ribo, M., & Pinz, A. (2001). A comparison of three uncertainty calculi for building sonar-based occupancy grids. *Robotics and Autonomous Systems*, *35*, 201–209.

Shafer, G. (1976). *A mathematical theory of evidence*. Princeton: Princeton University Press.

Silver, D., Morales, D., Rekleitis, L., Lisien, B., & Choset, H. (2004). *Arc carving : Obtaining accurate, low latency maps from ultrasonic range sensors* (pp. 1554–1561). In: Proceedings of the IEEE international conference on robotics and automation.

Thrun, S. (1998). Learning metric-topological maps for indoor mobile robot navigation. *Artificial Intelligence*, *99*(1), 21–71.

Thrun, S. (2003). Learning ocupancy grid maps with forward sensor models. *Autonomous Robots*, *15*, 111–127.

Thrun, S., Burgard, W., & Fox, D. (2002). *Probabilistic robotics*. Cambridge: MIT Press.

Zadeh, L. A. (1973). Outline of a new approach to the analysis of complex systems and decision process. *IEEE Transactions on Systems Man and Cybernetics*, *3*, 28–44.

Kyoungmin Lee received the B.S., M.S. and Ph.D. degrees in Mechanical Engineering in 2003, 2005, and 2009, respectively, from Pohang University of Science and Technology, Pohang, Korea. He is currently working as a Post Doctoral Researcher in Naval Postgraduate School, CA, USA. His research interests include the area of 3D simultaneous mapping and localization.

Se-Jin Lee received the B.S. degree in Mechanical Engineering from Hanyang University, South Korea, in 2003, and the M.S. degree and the Ph.D. degree from Pohang University of Science and Technology, Pohang, Korea, in 2005 and 2009 respectively. He is currently a professor at the Department of Applied Robotics, Kyungil University, Gyeongsan, Korea. His research interests are the sensor fusion and simultaneous localization and mapping (SLAM) for mobile robot navigation.

Mathias Kölsch has been working at the forefront of computer vision and image understanding for over a decade. He developed HandVu, the first visionbased hand gesture recognition system for realtime human-computer interaction. Recent efforts include building the "Computer Vision Algorithm Collection" to foster reuse and collaboration, and the "Easy! CV Library" to make Computer Vision more easily usable. Mathias received his Ph.D. from the University of California, Santa Barbara, in 2004. He is an Associate Professor of Computer Science at the Naval Postgraduate School in Monterey, CA, where he directs the NPS Vision Lab.

Wan Kyun Chung received his B.S. degree in Mechanical Design from Seoul National University in 1981, his M.S. degree in Mechanical Engineering from KAIST in 1983, and his Ph.D. in Production Engineering from KAIST in 1987. He is a professor in the school of Mechanical Engineering, POSTECH (he joined the faculty in 1987). In 1988, he was a visiting professor at the Robotics Institute of Carnegie-Mellon University. In 1995 he was a visiting scholar at the university of California, Berkeley. His research interests include the localization and navigation of mo-bile robots, underwater robots and development of robust controllers for precision motion control. He is a director of the National Research Laboratory for Intelligent Mobile Robot Navigation. He is serving as an Editor for IEEE Trans. on Robotics, and he is on the international editorial board for Advanced Robotics.